NANOSYSTEMS: PHYSICS, CHEMISTRY, MATHEMATICS, 2016, 7 (2), P. 340–348

An interpretation of the strongest X-ray diffraction peak for various carbon nanoclusters

A. V. Siklitskaya[1], S. G. Yastrebov[2], R. Smith[3]

[1]Institute of Theoretical Physics, University of Warsaw, Warsaw, Poland
[2]Ioffe Institute, St. Petersburg, Russia
[3]Loughborough University, Department of Mathematical Sciences, Loughborough, United Kingdom
Yastrebov@mail.ioffe.ru

PACS 61.05.C, 61.72.Dd, Ff **DOI 10.17586/2220-8054-2016-7-2-340-348**

The most intensive X-ray diffraction peaks for three types of carbon allotropes are analyzed: i) temperature-annealed nanodiamond powder (carbon "onions"), ii) multi-walled carbon nanotubes, iii) layers of epitaxial graphene. A reconstruction of the X-ray diffraction pattern using an intershell distribution, obtained by high resolution transmission electron microscopy, was compared to the XRD data. For a qualitative analysis of the diffraction profiles, the method of convolution of Lorentzians (size broadening profile), together with a statistical consideration of interlayer spacings (lattice strain broadening profile) were used. For the case of iii) the statistical distribution reduces to a Gaussian and the method itself transforms to a best fit procedure of the classical Voigt function to the experimental data. For cases i) and ii) and the high-resolution electron microscopy-reconstructed data, the method fits the experiment better using either negatively or positively -skewed statistical distributions, correspondingly. A model of particles with a spiral internal structure and with radius-dependent spacings between the successive turns may explain experimental data for these cases. The data for epitaxial graphene allows different interpretations, including fluctuations of lattice spacings caused by distortions of the valence bands and angles in the graphene planes or by the formation of scrolls.

Keywords: graphene, carbon onions, carbon, multiwalled carbon nanotubes, X-ray diffraction.

Received: 23 January 2016

1. Introduction

A study of the internal structure of new allotropic forms of carbon is important for the progress of materials science. In particular, obtaining information about the structure of materials and, therefore, their degree of perfection, helps to outline the areas for their practical applications. Thus, the study of structures that break the symmetry of graphitic planes is important for better understanding the practical realization of "theoretic" graphene as a material with a zero band gap and high electron mobility. In this paper, we present results of a qualitative analysis of the most intensive diffraction peak for several types of carbon allotropes constructed with sp^2-bonded atoms [1–4].

Because of graphene's unique geometry, there exists various possibilities for the modification of valence angles and bond lengths which change the structure; e.g. the Dienes (Stone-Wales) rearrangement [5]. Moreover, carbon polyhedra assembled with sp^2 bonds play an important role in the construction of nanoclusters having different shapes (e.g. carbon spheroids and spiroids).

It is very well known that X-ray diffraction (XRD) is the standard method for crystal structure analysis. However, allotropes such as graphene cannot be characterized by XRD because there is only a single (002) plane. For formation of the most intensive XRD peak,

similar to that for graphite, at least three planes are required [4]. Another problem with new allotropes of carbon is a lack of symmetry of the XRD profiles for carbon "onions", or, more strictly, for "temperature-annealed nanodiamond powder" [1], and for multi-walled carbon nanotubes (see, e.g. [2]). Here, we analyze the diffraction peaks for various carbon-based materials that belong to the region of XRD angles where peaks corresponding to those between (002) planes for crystalline graphite manifest themselves.

Usually line shape analysis of XRD peaks reduces to the realization of a best fit procedure for minimization of a functional, containing squares of sum of differences between experimental data and the convolution of a size- (commonly a Lorentzian (Cauchy) function) together with lattice strain broadening (commonly Gaussian) -profiles [6]. However, one may consider the lattice-strain profile as a statistical distribution different for the normal law without loss of generality. This statistical distribution can be asymmetric, e.g. negatively-skewed, as was shown by us for carbon onions obtained in the course of temperature annealing of nanodiamonds [1]. Here, we will also show that the negatively-skewed distribution will fit the XRD profile for multi-walled carbon nanotubes as well as for the carbon onions case. Moreover, we will demonstrate that for the case of a lattice-spacing distribution of a single carbon onion investigated by HRTEM [3], a statistical distribution with positive skewness will fit the experimental data. When a Gaussian distribution is used in the convolution, the resulting profile is termed Voigtian. Here, we will show that for the case of epitaxial graphite [4], a Voigt function fits the experimental diffraction profiles quite well.

2. Experimental and methodology

We accurately digitized data presented in papers [1–4]. The technological parameters of the manufactured samples are presented there. All XRD spectra were measured for CuKα radiation.

2.1. Formalism

The intensity of diffraction V as a function of double diffraction angle θ may be written in the following way:

$$V(\theta) = \int_{-\infty}^{\infty} S(\theta) L(\theta - \theta' - \theta_0) d\theta'. \tag{1}$$

Where θ_0 is doubled Bragg's angle, $S(\theta)$ is a statistical distribution function, $L(\theta)$ is Lorentzian (Cauchy function):

$$L(\theta) = \frac{2A}{\pi} \frac{w_L}{\theta^2 + w_L^2}. \tag{2}$$

Here, w_L is full width of the Lorentz's contour measured at its half height, and A is a constant. The parameter w_L is linked to Scherrer's equation:

$$D = \frac{K\lambda}{w_L cos(\theta_0/2)}, \tag{3}$$

and K is dimensionless constant that approximately equals to unity, $\theta_0/2$ is Bragg's angle. The equation (1) transforms to a Voigtian (Voigt function) when the function $S_s(\theta)$ follows the normal distribution (Gaussian) law:

$$S_s(\theta) = \sqrt{\frac{b}{\pi}} e^{-\theta^2 b}, \tag{4}$$

where $b = 4\ln(2)/w_G^2$ and w_G is full width of Gaussian contour measured at its half height. In this paper, we also modeled another statistical function, asymmetric, S_a. For its modeling we used a double sigmoidal law in the following form:

$$S_a(\theta) = \frac{1}{1+\exp\left(-\frac{\theta+\frac{w_1}{2}}{w_2}\right)}\left(1-\frac{1}{1+\frac{\theta-\frac{w_1}{2}}{w_3}}\right), \tag{5}$$

where w_1, w_2 and w_3 are parameters. For analysis of the intershell spacings in carbon onions obtained by analysis of HRTEM images, we used a probe function which was selected empirically:

$$\langle R(\delta r)\rangle = A_1 + \frac{A_1 - A_2}{1+\exp\left(-\frac{\delta r-\delta r_0}{\beta}\right)}, \tag{6}$$

where A_1, A_2, β, δr_0 are parameters, $\langle R_{\max}\rangle\, R(\delta r)$ is the mean radius of the shell: $\langle R(\delta r)\rangle \leq R_{\max}$; δr is a distance between two adjacent shells; $R_{\max}$ is the onion's outer radius.

One may introduce a function representing the distribution of intershell distances, $g(\delta r)$:

$$g(\delta r) = \frac{d\langle M(\delta r)\rangle}{d\delta r}, \tag{7}$$

where $\langle M(\delta r)\rangle$ is the mean number of intershell distances δr appearing in the interval $d\delta r$. On other hand, the following equation is also valid:

$$\langle R(\delta r)\rangle = \langle M(\delta r)\rangle \langle \delta r\rangle, \tag{8}$$

where δr is a mean intershell distance. One may calculate moments of the above distribution function (equation (7)) in the following way:

$$\langle M(\delta r)\rangle = \int_{\delta r_{\min}}^{\delta r} g(\delta r)d\delta r, \tag{9}$$

and

$$\langle \delta r\rangle = \int_{\delta r_{\min}}^{\delta r} \delta r g(\delta r)d\delta r. \tag{10}$$

Exploiting equation (8) and the assumption $g(\delta r) \sim \delta r g(\delta r)$, it easy to obtain the equation:

$$\langle R(\delta r)\rangle \approx \left(\int_{\delta r_{\min}}^{\delta r} g(\delta r)d\delta r\right)^2. \tag{11}$$

Thus:

$$g(\delta r) \approx \frac{\partial\left(\langle R(\delta r)\rangle^{1/2}\right)}{\partial \delta r}. \tag{12}$$

2.2. Analysis of experimental data

2.2.1. Annealed nanodiamonds and multiwalled carbon nanotubes. Figure 1 presents the XRD pattern for temperature-annealed nanodiamonds [1]. It is negatively-skewed. We met a difficulty finding a unique selection of the symmetric component for the results presented in the Fig. 1 and so used equations (1), (2) and (5) for a single negatively-skewed profile. The result of the calculation is depicted by the continuous curve. Parameters were obtained by the least squares fitting technique. The asymmetry of the internal structure of the onion may result in the skewness. A sketch of the cross section of such an onion is presented in the inset. Such kind of spiral onions were termed as carbon spiroids [7]. In the particular case presented here, the radius of the spiral turn depends irregularly on the spacing between successive turns. The principal role of such spiroidal particles in the formation of the XRD profile may reflect their prevailing number in a comparison to 'deal' spheroids.

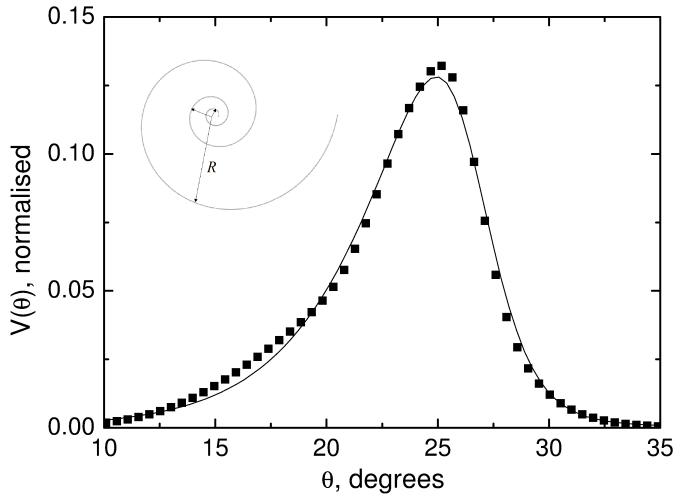

FIG. 1. The XRD profile for a powder of nanodiamonds transformed to onions by annealing. The black squares and solid contour show experimental data from [1] and the result of calculation with equations (1), (2) and (5) , correspondingly for $w_1 = 0°$, $w_2 = 3.11°$, $w_3 = 1.01°$, $w_L = 0.5°$. The insert shows a schematic of the equatorial section of a spiroidal particle (spiroid).

A slightly different situation occurs in the case of multi-walled carbon nanotubes. Fig. 2 shows XRD profile for the nanotubes. One may see the result of decomposition of the experimental data [2] on two contours. One is asymmetric ([equations (1), (2) and (5)]; the curve marked by number 1) and the second one is symmetric (Voigtian [equations (1),(2) and (4)]; curve 2). By analogy with carbon spiroids, we may term nanotubes contributing to contour (1) as spirocylindroids. A sketch of the cross-section of a spirocylindroid is presented in the insert to Fig. 2. In this case there is no principal role played by spiroidal particles to the XRD profile which may reflect a contribution from 'ideal' nanotubes that is comparable with the contribution of the spirocylindroids.

2.2.2. Carbon onions. Here, we interpret the experimental data from paper [1] where the dependence of the distances between successive shells of the carbon spheroids are presented as a function of the shell's radius. The inverse function is portrayed in Fig. 3. For simplicity, we kept symbols marking experimental points similar to ones presented in [1]. The full line marked by number 1 represents data calculated with equation (6) and the triangles illustrate

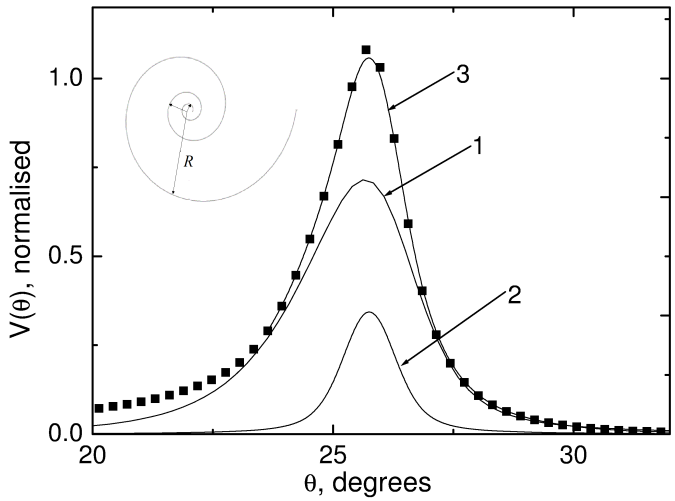

FIG. 2. The XRD profile for multi-walled carbon nanotubes. The black squares portray experimental data from [2]; the curve marked by number 1 presents results of calculation with equations (1), (2) and (5) with the following parameters: $w_1 = 0°$, $w_2 = 2°$, $w_3 = 0.456°$, $w_L = 1°$, $A = 0.43$. The line marked by number 2 shows the calculation with equations (1), (2) and (4) for $\theta_0 = 25.75°$, $A = 0.178$, $w_G = 0.87°$,$w_L = 0.633°$ ("ideal" nanotube). Curve 3 is the sum of curves (1) and (2). The insert shows a schematic of the cross section of a spirocylindroid.

equation (12). The full line connecting the triangles is the Gaussian approximation. Therefore, the obtained distribution is symmetric. However, it is easy to see in Fig. 4 that after conversion of the intershell distances to the double diffraction angles with the help of Bragg's law, the resulting dependence is no longer symmetric and is positively-skewed. This characterizes the lattice strain function. To use the lattice strain function in equation (1), one has to shift the argument values to the left, starting the new argument zero point from the position of the maximum. The parameter w_L was calculated using equation (3) using data of the diameter of carbon onions from [3] and the CuKα radiation wavelength. The resulting convolution of the lattice strain and Lorentzian profiles are presented in Fig. 4 by open circles. Such dependences characterize the internal structure of the carbon onion. Obviously, while the area of larger angles characterizes the central part of the onion, where some compression of the lattice spacings was observed [3], the region for smaller angles characterizes its peripheral region. It is natural to attribute such behavior to a spiroid with lattice spacings expanding from central to peripheral area. It seems obvious to draw similar conclusions about the behavior of lattice spacings for the cases considered above. However, the degrees of expansions are different. For cases of Figs. 1 and 2, the diffraction profiles are negatively skewed, meaning a faster drop of the function in the smaller intershell distances region and a slower drop in the larger intershell distances region.

An estimation of Scherrer's size for thermally annealed nanodiamonds and multi-walled nanotubes (see captions to Fig. 1 and Fig. 2 and equation (3)), i.e. ~ 14 nm, indicates the formation of relatively large clusters. These may appear for the case of thermally-annealed nanodiamonds because this size is sufficiently larger than the mean size of pristine nanodiamonds (~ 4 nm). The cluster enlargement may appear because of single cluster aggregation to bigger particles. However we cannot extend this result to nanotubes because of a lack of information about their origin. In this case of aggregation to the resulting "lattice strain" profile may transform to statistics of lattice spacings in larger clusters with more complex structures.

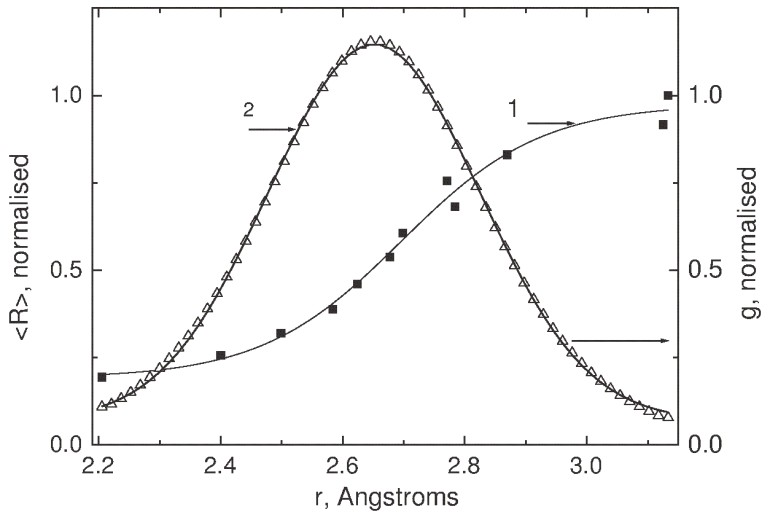

FIG. 3. The black squares give the experimental dependence of a shell's radius normalized to the external radius of a multishell carbon spheroid (carbon "onion") as a function of the intershell distances, as published in [3]. The continuous line 1 represents an approximation of the experimental data using equation (6) with the following set of parameters: $A_1 = 0.19 \pm 0.03$, $A_2 = 0.97 \pm 0.03$, $\delta r_0 = 2.696 \pm 0.016$ Å, $\beta = 0.11 \pm 0.02$ Å. The triangles give results for the calculation of the distribution function using equation (12); the full line shows the Gaussian fit.

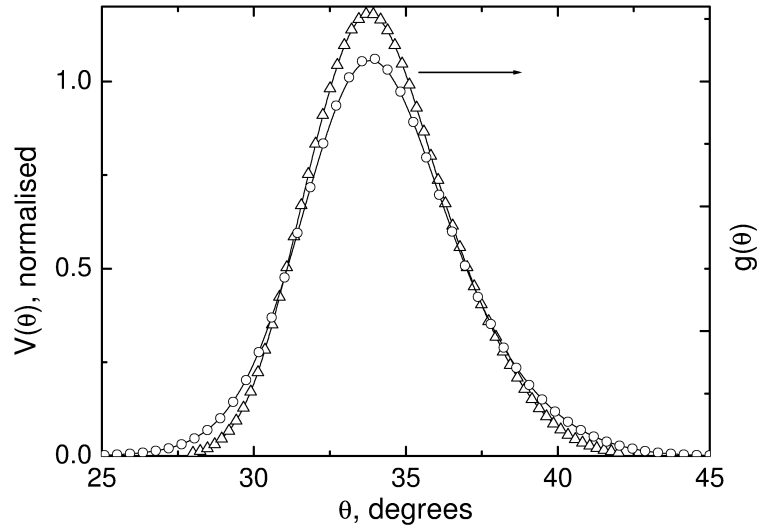

FIG. 4. The lattice strain function $g(\theta)$ of intershell spacings for a carbon multishell particle plotted versus the diffraction angle is given by triangles after conversion of the spacings to double diffraction angles by Bragg's law. Circles depict results of the calculation with equation (1) with the diffraction profile from a shifted lattice strain function. Here, for calculation of the XRD profile, the following parameters were used: $\theta_0 = 33.98^\circ$ is position of the maximum and the parameter $w_L = 0.6^\circ$ is calculated with Scherrer's equation (3) for the actual cluster diameter (see paper [3]).

2.2.3. Epitaxial graphite. The experimental data for epitaxial graphite together with their fit by a Voigtian function are collected in Fig. 5 [4]. One may see a good agreement between the model and experimental data for all cases presented in Fig. 5. Two possible versions of graphene flaks deformation are presented in the insets- $sine$ and $cosine$ types of distortions (the left inset to Fig. 5) and formation of scrolls (spirocylindroids). A similar effect of transformation of material from graphene to scrolls has been presented in paper [8]. The distortion of the graphene planessymmetries results in the annihilation of their valuable properties such as zero effective mass and high mobility of charge carriers. Fig. 6 shows the width of the lattice strain profile vs substrate material and technology of deposition. One can clearly see that all grown layers are distorted. The lesser distorted sample is graphite obtained by the thermal decomposition of SiC. The parameter $w_L \to 0$ is only for the profile marked in Fig. 5 by by triangles. It means that size of graphite fragment is large enough to be estimated by Scherrer's formula (equation 3) and the Voigtian transforms to a Gaussian. Only the lattice strain profile is available from the experiment. Fig. 7 presents Scherrer's diameter for a cluster of epitaxial graphite grown on different substrates, calculated using w_L from the caption to Fig. 5.

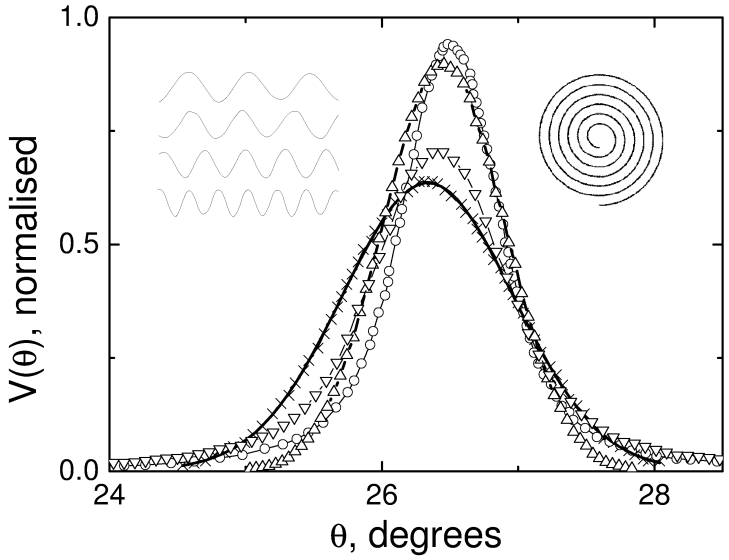

FIG. 5. A Voigtian fit of experimental diffraction profiles for epitaxial graphite [4]. Different symbols stand for different substrates. The continuous line presents results of the best fit. 1. The inverted triangles correspond to epitaxial graphite grown by CVD on the surface C 6H–SiC: $\theta_0 = 26.42^\circ \pm 0.002$, $A = 1.09 \pm 0.003$, $w_G = 0.81 \pm 0.01^\circ$, $w_L = 0.601 \pm 0.01$. 2. The inclining crosses give the thermal decomposition of the surface C 4H–SiC: $\theta_0 = 26.33 \pm 0.002^\circ$, $A = 1.012 \pm 0.005$, $w_G = 1.465 \pm 0.014^\circ$, $w_L = 0.034 \pm 0.02$. 3. The circles represent the thermal decomposition of the surface C 6H–SiC: $\theta_0 = 26.51 \pm 0.001^\circ$, $A = 1.07 \pm 0.004$, $w_G = 0.57 \pm 0.01^o$, $w_L = 0.465 \pm 0.01^\circ$. 4. Triangles – CVD grown epitaxial graphite grown by CVD on substrate Si–SiO_2–Ni: $\theta_0 = 26.45 \pm 0.001^\circ$, $A = 1.000 \pm 0.0004$, $w_G = 1.04 \pm 0.001^\circ$, $w_L = 0$. Insets show two modes of deformation for the graphene planes: left – sine (cosine) through formation of Dienes (Stone-Wales) defects and right – through formation of spirocylindroids.

.

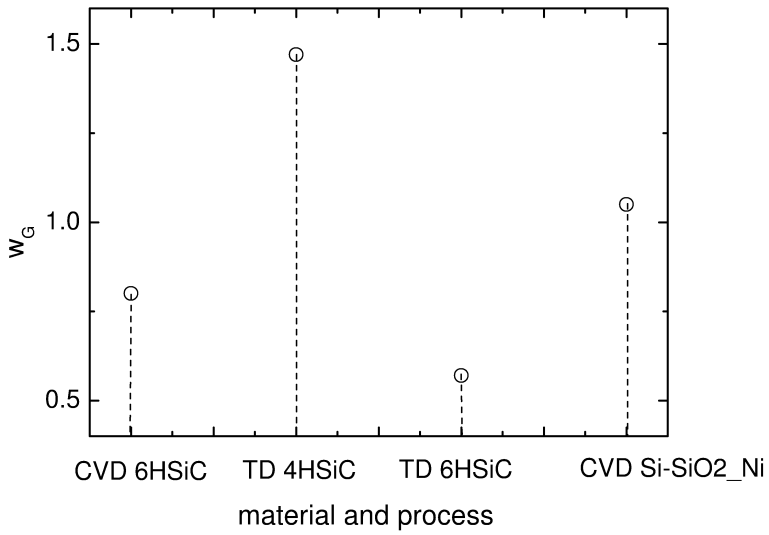

FIG. 6. The parameter w_G calculated by the best fit procedure from results presented in Fig. 5 for different materials

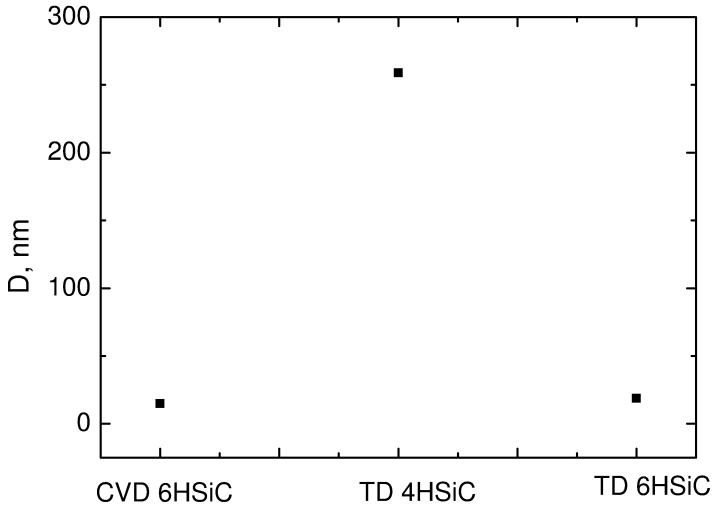

FIG. 7. Scherrer's diameter calculated from equation (3) and parameters w_L presented in the captions to Fig. 5 for different substrate materials and technologies

3. Conclusions

The estimations performed in this paper lead to two preliminary conclusions:

1. The spiroid-spirocylindroid model of a particle with interturn distances expanding from center of the particle to its peripheral area fits experimental data for carbon onions and multi-walled carbon nanotubes quite well.
2. Spiroidal models might not be unique.
3. XRD study reveals a distortion of the symmetry of graphene planes for the epitaxial-grown graphite clusters.

4. The distortions break the symmetry of graphene planes and, therefore, may affect negatively charge transport properties.
5. A lack of profiles for a single graphene layer makes it difficult to standardize XRD for this material.

References

[1] Mykhaylyk O. O., Solonin Y. M., Batchelder D. N. et al. Transformation of nanodiamond into carbon onions: A comparative study by high-resolution transmission electron microscopy, electron energy-loss spectroscopy, x-ray diffraction, small-angle X-ray scattering, and ultraviolet Raman spectroscopy. *Appl. Phys.*, 2005, **97**, 074302, 16 pp.

[2] Shah N. A., Abbas M., Amin M. et al. Design and analysis of functional multiwalled carbon nanotubes for infrared sensors. *Sensor Actuat A-Phys.*, 2013, **203**, P. 142–148.

[3] Banhart F., Ajayan P. M. Carbon onions as nanoscopic pressure cells for diamond formation. *Nature*, 1996, **382**, P. 433–435.

[4] Tokarczyk M., Kowalski G., Kepa H. et al. Multilayer graphene stacks grown by different methods-thickness measurements by X-ray diffraction, Raman spectroscopy and optical transmission. *Crystallogr. Reports*, 2013, **58**(7), P. 1053–1057.

[5] Ma J. Stone-Wales defects in graphene and other planar sp^2-bonded materials. *Phys. Rev.B*, 2009, **80**, 033407, 4 pp.

[6] Langford J. L, Delhez R., de Keijser Th., et al. Profile Analysis for Microcrystalline Properties by the Fourier and Other Methods. *Aust. J. Phys.*, 1988, **41**, P. 173–181.

[7] Ozawa M., Goto H., Kusunoki M. Continuously Growing Spiral Carbon Nanoparticles as the Intermediates in the Formation of Fullerenes and Nanoonions. *Phys. Chem. B*, 2002, **106**, P. 7135–7138.

[8] Zilong Liu Z., Qingzhong X., Tao Ye. Carbon nanoscroll from C_4H/C_4F-type graphene superlattice: MD and MM simulation insights. *Phys. Chem. Chemi. Physics*, 2015, **17**(5), P. 3441–3450.